Volume 14
Number 3
21 January 2022
Pages 549-1020

Nanoscale

rsc.li/nanoscale

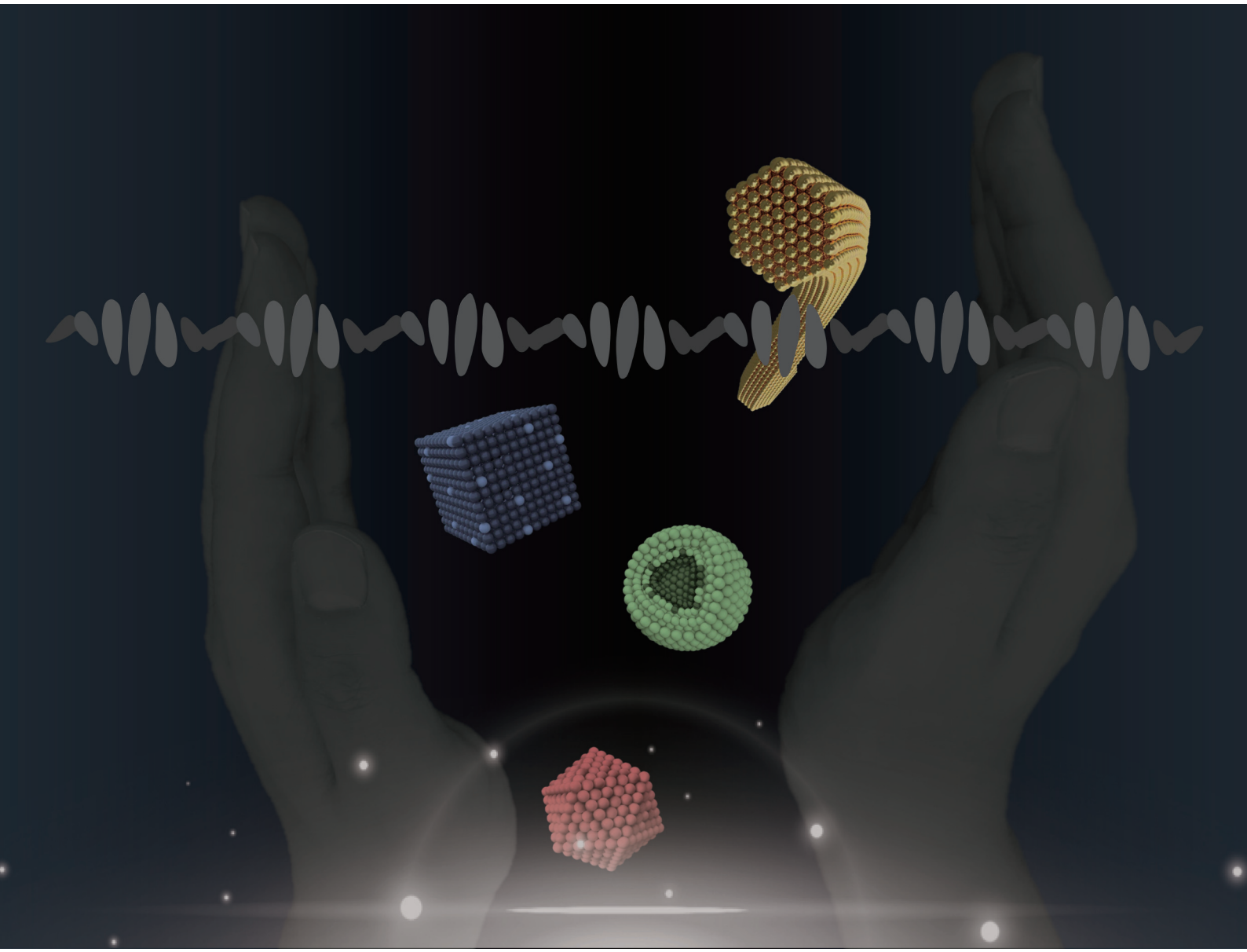

ISSN 2040-3372

ROYAL SOCIETY OF CHEMISTRY

MINIREVIEW
Taotao Zhuang *et al.*
Amplifying inorganic chirality using liquid crystals

NCNST

Nanoscale

ROYAL SOCIETY OF CHEMISTRY

MINIREVIEW

View Article Online
View Journal | View Issue

Cite this: *Nanoscale*, 2022, **14**, 592

Amplifying inorganic chirality using liquid crystals

Mingjiang Zhang,†[a] Yaxin Wang,†[a] Yajie Zhou,[a] Honghan Yuan,[a,b] Qi Guo[a] and Taotao Zhuang *[a]

Received 14th September 2021,
Accepted 14th November 2021

DOI: 10.1039/d1nr06036h

rsc.li/nanoscale

Chiral inorganic nanostructures have drawn extensive attention thanks to their unique physical properties as well as multidisciplinary applications. Amplifying inorganic chirality using liquid crystals (LCs) is an efficient way to enhance the parented inorganic asymmetry owing to chirality transfer. Herein, the universal synthetic methods and structural characterizations of chiral inorganic-doped LC hybrids are introduced. Additionally, the current progress and status of recent experiment and theory research about chiral interactions between inorganic nanomaterials (*e.g.* metal, semiconductor, perovskite, and magnetic oxide) and LCs are summarized in this review. We further present representative applications of these new hybrids in the area of encryption, sensing, optics, *etc*. Finally, we provide perspectives on this field in terms of material variety, new synthesis, and future practice. It is envisaged that LCs will act as a pivotal part in the amplification of inorganic chirality with versatile applications.

1. Introduction

Chiral nanostructures, referring to the mirror images that cannot superimpose with the original ones at the nanoscale, have drawn great attention on account of their promising applications in enantioselective separation,[1] optoelectronic devices,[2] chiral sensors,[3] 3D display,[4] chiral catalysis,[5] *etc*. The chirality of nanomaterials is commonly observed by their optical activity, manifested by various studies, such as circular dichroism (CD) and circularly polarized luminescence (CPL).[6–8] CD represents the different absorption of left-handed and right-handed light when circularly-polarized light passes through chiral components. Generally, the anisotropic factor (*g*-factor) is used for the quantitative analysis of chiroptical activity, which is defined as $g = \Delta\varepsilon/\varepsilon = (\varepsilon_L - \varepsilon_R)/(\varepsilon_L + \varepsilon_R)$, where $\Delta\varepsilon$ is the difference in molar absorptivity, ε is molar absorptivity, and ε_L and ε_R are the absorptivity to left-handed and right-handed circularly-polarized light, respectively. CPL refers to the different-handed circularly polarized light emitted from the chiral luminescent system. The luminescence dissymmetry factor (g_{lum}) is used to quantify the magnitude of CPL, and $g_{lum} = 2 \times (I_L - I_R)/(I_L + I_R)$, where I_L and I_R are the intensities of left-handed and right-handed circularly polarized light

[a]*Division of Nanomaterials & Chemistry, Hefei National Laboratory for Physical Sciences at the Microscale, Department of Chemistry, University of Science and Technology of China, Hefei 230026, China. E-mail: tzhuang@ustc.edu.cn*
[b]*Ganjiang Innovation Academy, Chinese Academy of Sciences, Ganzhou 341000, China*
† Co-first authors.

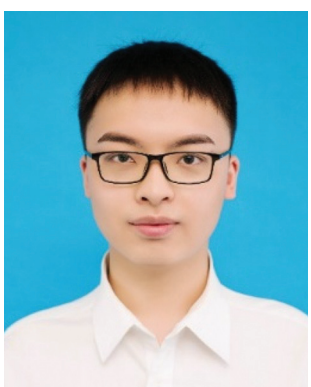

Mingjiang Zhang

Mingjiang Zhang is currently a graduate student under the supervision of Prof. Taotao Zhuang at University of Science and Technology of China. His recent research focuses on chiral liquid crystals, circularly polarized luminescence, and related applications.

Yaxin Wang

Yaxin Wang is currently a graduate student under the supervision of Prof. Taotao Zhuang at University of Science and Technology of China. Her ongoing research includes chiral nanocrystalline cellulose film, circularly polarized luminescence, and related applications.

emitted by chiral materials, respectively.[9] Currently, chiral organic small molecules are dominating research objects in the chiral material synthesis and applications because they not only have simple and clear molecular structures but also possess a wide variety and are easy to be derived.[10,11] Unfortunately, these chiral organic molecules are mainly based on various proteins or complex chemical frameworks, resulting in high cost of synthesis, extraction, and purification.[12] In practical applications, materials with high *g*-factor or g_{lum} values are demanded, but most chiral organic materials are difficult to meet the requirements.[13,14]

Meanwhile, chiral inorganics have been regarded as emerging candidates owing to their intense light–matter interactions.[15,16] However, the current usual strategy to endow inorganic chirality – capping chiral ligands – limits the *g*-factor or g_{lum} value within the range of 10^{-4}–10^{-3}.[17,18] The values are far away from practical demand, urgently needing amplification. Additionally, some alternative strategies have been reported towards the amplification of chirality in the nanomaterial system. For example, supramolecular self-assembly, an efficient and simple strategy, can arrange individual inorganic nanomaterials into ordered structures.[19–22] Tang *et al.* organized Au clusters with CD but free of CPL into a uniform body-centered cubic packing assembly, realizing remarkably amplified CD intensity along with the appearance of the CPL signal.[23] Besides, plasmon resonance can significantly enhance the chiroptical properties of molecules around metallic surfaces because of the interactions between photons and electrons at the surface of noble metals.[24–28] Mishima *et al.* proposed the example of using Ag nanoparticles to enhance the CPL properties of *meso*-tetrakis-(4-sulfonatophenyl)porphyrin-cationic-surfactant complexes.[29]

Recently, an intriguing approach for amplifying chirality through the co-assembly pathway, namely, the sergeant-soldier rule, has been widely demonstrated.[30] Using small amounts of chiral dopants (*i.e.*, the sergeant) enables a helical twist in large volumes of achiral molecules (*i.e.*, the soldier), which is an efficient way to enhance the parented inorganic asymmetry.[31,32] This approach offers a stage to detect and quantify nanomaterial chirality, as well as providing the huge potential for future applications and developments.

Liquid crystals (LCs), the anisotropic, partially ordered fluids, possess long-range orientational order and show some fascinating properties.[33] They are sensitive to the perturbation of chiral dopants, and thus leading to chiral amplification.[34] The addition of chiral dopants to nematic LCs induces the formation of chiral nematic LCs (N*LCs).[35] N*LCs are one kind of quasi-one-dimensional photonic crystals, which have gained much interest thanks to their fantastic optical properties towards chirality enhancement, as well as their universal applicability when combining inorganic materials.[36–38] Enhanced chirality can be credited to a chirality transfer process from the molecular level to macrolevel, within the formation of N*LCs.[39]

Amplifying inorganic chirality by LCs is a new and fantastic research field, but faces many challenges, particularly the comprehensive understanding of chirality transfer. Thus, this mini-review will focus on chiral interactions between inorganic nanomaterials (*e.g.*, metal, semiconductor, perovskite, and magnetic oxide) and LCs. Herein, the recent progress of experiment and theory researches, fabrication method, characterization, and practical application about chirality enhancement of nanomaterials by inducing LCs will be presented.

2. Fabrication and chirality evaluation of N*LCs

As quasi-one-dimensional photonic crystals, N*LCs were used to generate and amplify the chirality of nanomaterials thanks to their fantastic optical properties and excellent versatility.[38,40] The formed N*LCs possess periodic helical structures and can be confirmed by the typical fingerprint textures photographed using polarized light optical microscopy.[41] Here, we will introduce the general fabrication strategies and the most essential parameters for the chirality assessment of N*LCs.

2.1 Fabrication strategies

The properties exhibited by hybrid N*LC systems are consistent with their fabrication methods; herein, only inorganic dopants are discussed. As long as one component is chiral, the chirality of the hybrid systems can be induced, whether the inorganic dopants are chiral or not. Thus, a wide range of hybrid N*LCs can be produced by molecular design and assembly. The general fabrication strategies of N*LCs will be introduced as follows (Scheme 1). Initially, if the host LCs are chiral, N*LCs could serve as chiral sources, enabling other achiral inorganic components to encapsulate or incorporate into the chiral LC host.[42] On this occasion, the embedded part possesses unique physical functions such as photoluminescence and magnetism. For example, inorganic emitters with high photoluminescence quantum yield often function as inorganic dopants. To obtain CPL with large g_{lum} values, the inorganic

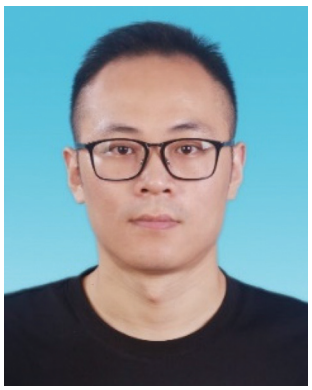

Taotao Zhuang

Taotao Zhuang received his Ph.D degree in inorganic chemistry from the University of Science and Technology of China and then worked as a postdoc fellow at the University of Toronto. He was appointed as a professor in 2020 at University of Science and Technology of China. Now he is challenging to synthesize new inorganic chiral nanomaterials, understand the mechanism of structure–property, and realize the practical applications using home-made materials.

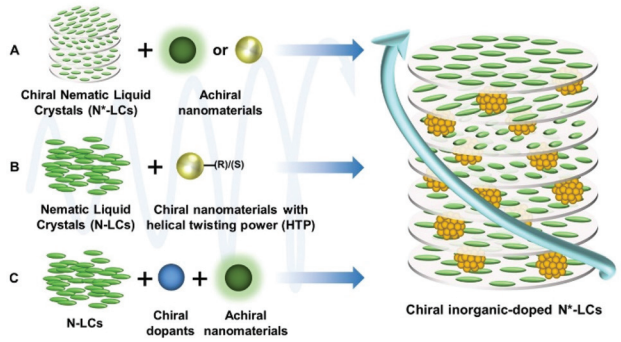

Scheme 1 Schematic illustration of the synthetic fabrication of inorganic-doped N*LCs. (A) Encapsulating or incorporating achiral nanomaterials into chiral LCs host. Achiral nanomaterials include emissive dopants and non-emissive dopants, which are represented by green and yellow balls, respectively. (B) Using chiral nanomaterials with strong helical twisting power (HTP) to induce chirality in achiral nematic liquid crystals (N-LCs) directly. (C) Combining achiral nanomaterials and N-LCs with extra addition of chiral dopants.

emitters are always located at the centre of the photonic bandgap (PBG). However, the fluorescence intensity emitted by the systems would be depressed because the light wavelength at the centre of PBG cannot propagate through the photonic crystals. On the contrary, when locating inorganic emitters at the edge of PBG, the fluorescence intensity will be enhanced because the light passes through it at a reduced group velocity owing to the resonant Bragg scattering. CPL will always occur because N*LCs provide chiral hosts for inorganic emitters. Thus, designing the system properly to gain both large g_{lum} values and high emission intensity is extremely important. Furthermore, when inorganic components are chiral, as well as being capable of twisting the helixes of LCs, the inorganic phases can directly function as chiral dopants to induce the helix structure in achiral LCs.[43] In this case, the chirality will be transferred from functional nanomaterials to surrounding LCs, as a consequence of which, the overall chirality will be amplified by several orders of magnitude. Additionally, if host LCs are achiral, while the incorporated inorganic functional nanomaterials have no ability to induce chirality, the extra addition of chiral dopants is necessary to form N*LCs.[44] Similar to the first case, the induced N*LCs provide a chiral environment for the functional components.

2.2 Critical parameters

The key factor for chirality amplifying *via* N*LCs is to form helical structures, induced by the chiral dopants in the LC matrix. Handedness, as well as helical pitch, are the most commonly used parameters that are used to characterize the N*LC system.

2.2.1 Handedness. Handedness stands for the direction in which the molecular rotates along the spiral axis, including the left- and handed-rotations.[45] The handedness of N*LCs is determined by the configuration of chiral dopants interacting with the LCs, independent of chiral dopants' handedness. The handedness is evaluated by the Cotton effect, which is measured by CD or CPL spectra commonly. For a typical CD or CPL spectroscopy, the positive signal symbolizes the left-handed rotation, while the negative signal is corresponding to the right-handed one. When blended with chiral dopants, N*LCs will form a helical structure by self-organizing, manifested as the selective Bragg reflection of lights. CPL with the same rotation as the N*LCs is reflected, while CPL with the opposite rotation is transmitted.[46]

2.2.2 Helical pitch. Pitch (p) is defined as the distance of 360° rotation of the helix, representing the degree of spatial interactions between chiral dopants guest and N*LC host, which can be calculated by[47,48]

$$p = 1/(\beta ee \cdot c),$$

where β refers to the helical twisting power (HTP), which, represents the ability of chiral dopants to induce the formation of helical structures in achiral LC host.[49] ee refers to the enantiomeric excess, and c refers to the molar concentration. The helical pitch of N*LCs is commonly determined by the Grandjean-Cano wedge cell method.[44] It can be adjusted by the number of chiral dopants, external stimuli, including heat, magnetic field, and electric field.

3. Inorganic chirality generation and amplification in N*LCs

The combination of inorganic components and N*LCs will bring many fantastic properties. The induced N*LC phase turns out to be an excellent host, providing a chiral environment for inorganic nanomaterials to generate and amplify chirality. Understanding the generation and amplification mechanisms of chirality is essential for designing new chiral materials based on N*LCs. In this section, four main kinds of inorganic dopants will be discussed, including metal, semiconductor, perovskite, and magnetic oxide.

3.1 Metal

LCs are highly suitable candidates for studying the mechanism of chirality transfer from chiral molecules or interfaces to the surrounding environment. Chiral plasmonic nanomaterials are capable of achieving adjustable chiral photoelectric performance, precisely regulating chirality transfer and amplifying the system chirality.[50,51] A vital issue to be addressed is how far the chirality transfer is from a chiral matrix, especially a chiral nanoscale surface, to the bulk, and whether the shape or size of the nanoscale surface matters. As illustrated in Fig. 1A–D, Taizo Mori *et al.* synthesized gold nanoparticles capped with three different chiral ligands and varying in size, curvature and ligand density, to regulate chirality transfer from the surface of nanoparticles to the bulk LC medium.[52] They proposed that the helicity and chirality transfer efficiency of axial chiral binaphthyl derivatives can be controlled by the surface of metals and finally achieve precise regulation. Anshul Sharma *et al.* used cholesterol ligand to synthesize

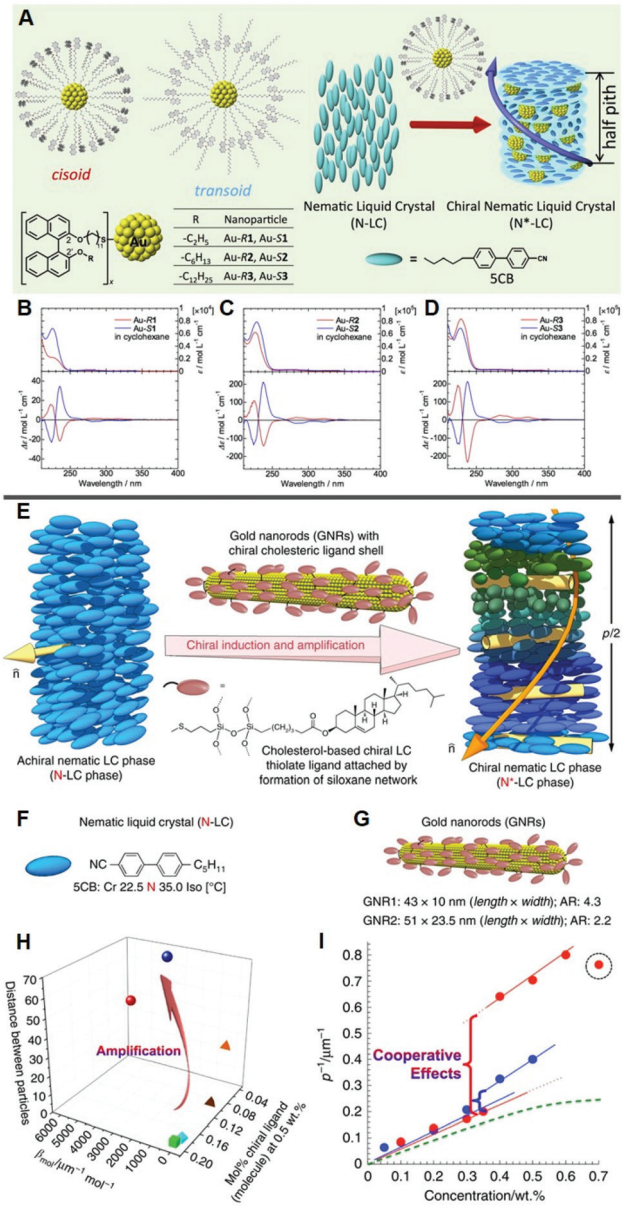

Fig. 1 (A) Illustration of the hybrid N*-LC structure with addition of the axially chiral binaphthyl-capped Au nanoparticles. (B)–(D) UV-vis and CD spectra of the chiral Au in cyclohexane for Au–R1 and Au–S1, Au–R2 and Au–S2, Au–R3 and Au–S3, respectively. Adapted with permission from ref. 52. Copyright 2016, American Chemical Society. (E) Illustration of chirality amplified by doping small amounts of chiral gold nanorods into the LC host. (F) The structure of LC 5CB. (G) The structure and size of Au nanorods. (H) Comparison of chiral transfer efficiency. (I) Relationship between p^{-1} (μm^{-1}) and the concentration (wt%) of Au nanorods. Adapted with permission from ref. 43. Copyright 2018, Springer Nature.

chiral gold nanoparticles. They prepared a uniform chiral nematic LC system for the detection, understanding, and visualization of chirality transfer from inorganics to the surrounding bulk.[53]

Obtaining a high dissymmetry factor is an essential issue in studying chiral materials. In general, molecules close to the plasmonic surface will exhibit plasmon enhancement, enabling enhanced electromagnetic field and exciton plasmon coupling. Since the surface plasmon resonance effect of metal nanomaterials can significantly amplify the chirality of surrounding chiral species, it is deserved to the extent that the chirality amplification is based on surface plasmon resonance systems. As illustrated in Fig. 1E–I, researchers designed a powerful method to realize chiral amplification *via* desymmetrization of plasmonic nanoparticles to nanorods.[43] Combing the chiral molecules with Au nanorods induces a tighter spiral distortion in the host LC, achieving a significant amplification of the hybrid chirality.[54]

3.2 Semiconductor quantum dot

Colloidal semiconductor quantum dots (QDs) display a unique quantum confinement optical effect in UV-visible-NIR wavelength with extensive tunability, high photostability, high quantum yields, and other properties.[55] Notably, by imparting chirality or constructing a chiral environment in the QD system, vigorous chiroptical activity such as absorption and emission of circularly polarized light at the wavelength corresponding to the exciton transitions could be achieved.[56,57] Many research works on the hybrid systems, composed of inorganic QDs and N*LCs, are emerging and showing the combined advantages such as flexible tunability and high stability. In 2011, Shibaev *et al.* chose CdSe/ZnS QDs as fluorescent dopants and prepared cholesteric fluorescent systems by doping glass-forming photoactive cholesteric LCs, preliminarily demonstrating the properties of optical tunability of CPL.[58] It should be noted that it is the first report using inorganic semiconductor QDs as emitters in chiral hybrids. After that, Nabiev *et al.* developed polymer-stabilized LC materials with a wide PBG by doping CdSe/ZnS QDs and chiral photochromic dopants, realizing the selective light reflection of CPL, as well as the tunable g_{lum} values *via* conformational changes in the helix structure of N*LCs.[59] Ghosh *et al.* embedded QDs into a one-dimensional N*LC photonic cavity and achieved the selective CPL enhancement by overlapping the emission of QDs with the edge of the stopband.[44]

In recent years, the cellulose nanocrystal (CNC) photonic films have also been demonstrated to be extraordinary chiral hosts for the organization of semiconductor nanomaterials due to their chiral nematic structures.[60] Functional CPL-active materials can be constructed by inducing semiconductor nanocrystals (NCs) into the CNC, reflecting CPL with left-handedness and emitting right-handed one because of its inherent left-handed helical structure.[61,62] As illustrated in Fig. 2A–C, Liu *et al.* induced CdSe/ZnS QDs into self-assembled chiral photonic CNC films to realize both left-handed CPL reflection and right-handed CPL emission with full-color tunable wavelengths.[63] A superior $|g_{lum}|$ value of 0.31 was achieved by tailoring the overlap between the PBGs and the emission of QDs with an additive of glycerol. In the same way, Sun *et al.* realized the CPL-active solid films by co-assembling CdSe/CdS quantum rods with the left-handed CNC templates.[64] Through the electrostatic repulsion of cellulose nanocrystals in the

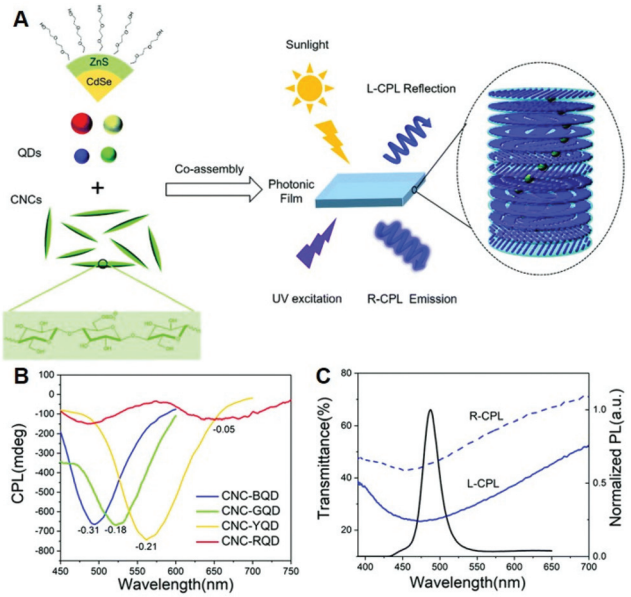

Fig. 2 (A) Illustration of R-CPL emission and L-CPL reflection by co-assembling ZnS/CdSe QDs with CNCs. (B) CPL spectra of QDs-doped CNC photonic films. (C) Transmission spectra of hybrid CNC films and photoluminescence spectra of QDs dispersion. Adapted with permission from ref. 63. Copyright 2019, Royal Society of Chemistry.

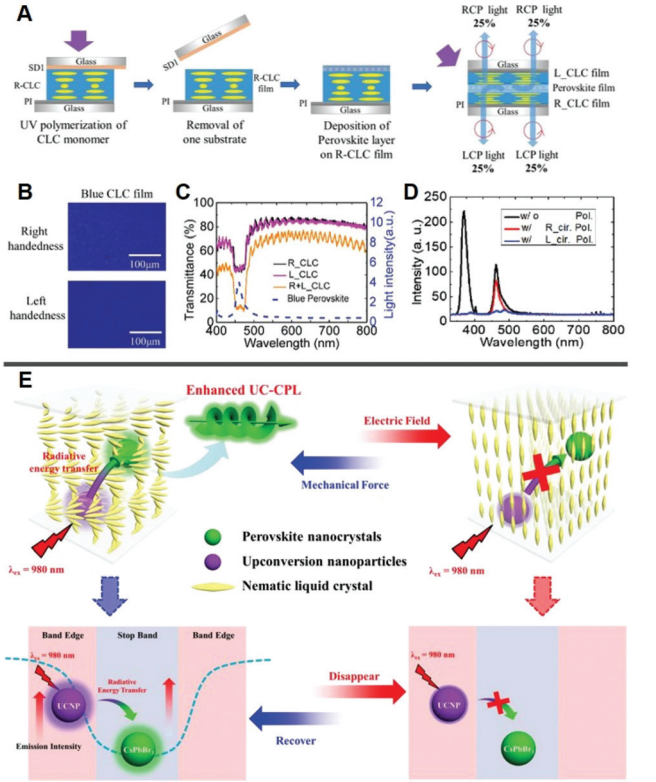

Fig. 3 (A) The fabrication progress of N*LCs stacked perovskite NCs. (B) POM images of N*LCs films with left- and right-handedness. (C) Transmittance spectra of N*LCs film. (D) Photoluminescence spectra of the CPL system with and without polarizing filters. Adapted with permission from ref. 68. Copyright 2019, Wiley-VCH. (E) Appropriate amounts of $CsPbBr_3$ NCs and upconversion nanoparticles were incorporated into N*LCs, enabling upconverted CPL by the radiative energy transfer process with a voltage-force regulated switch. $CsPbBr_3$ NCs and upconversion nanoparticles were located at the centre and edge of PBG of N*LCs, respectively, to achieve both high g_{lum} values and emission intensity. Adapted with permission from ref. 70. Copyright 2020, Wiley-VCH.

aqueous suspension, the PBG was adjusted to be overlapping with the photoluminescence bandgap, resulting in a $|g_{lum}|$ value as high as 0.45. This work extended the semiconductor fluorescent dopants from zero-dimension to one-dimension.

3.3 Perovskite

Halide perovskites have specific advantages such as narrow-band emission peak, high photoluminescence quantum yield, and wavelength tunability, and thus leading to attractive CPL when combined with a chiral host.[65,66] Constructing perovskites-doped N*LC system is an efficient way to avoid luminescent quenching induced by the ligand.[67] As presented in Fig. 3A–D, chirality can be introduced into perovskite NCs by stacking N*LCs with predefined handedness onto the surface of inorganic perovskites.[68] By using the N*LC film as a selective filter, CPL with a large g_{lum} value of 1.6 was transformed from the unpolarized light emitted by perovskites NCs. When stacking the perovskite layer on the N*LC film with right-handedness, the upward light reflected right-handed CPL while the downward light emitted left-handed CPL after across the N*LC films. Taking the L-CPL for example, the half of L-CPL passes through the R-handed N*LCs directly, while the rest is reflected by the L-handed N*LCs and followed by passing through the R-handed N*LCs. It works as the same way for R-CPL. Fully chiral light luminescence can be achieved with a 100% circular polarization conversion efficiency in theory because of the selective reflection of N*LC films.

Additionally, N*LC matrix-doped with perovskite nanocrystals and upconversion nanoparticles can be used to enhance the upconverted CPL.[69] When $CsPbBr_3$ NCs were adjusted to the center of the PBG of N*LCs, the CPL activity can be obtained in this system, as well as a large g_{lum} value (Fig. 3E).[70] Moreover, by locating the emission spectra of upconversion nanoparticles at the edge of the PBG, the upconverting emission has been significantly enhanced. In this case, $CsPbBr_3$ NCs reabsorbed the enhanced emission of upconversion nanoparticles and thus improved the emission of $CsPbBr_3$ NCs by radiative energy transfer. In other words, a large g_{lum} value of 1.1 and enhanced emission was achieved by steering the PBG.

3.4 Magnetic oxide

One of the most outstanding properties of LCs is the distribution of the optical axis in the LC layer and can be regulated by an external electric or magnetic field, and thus controlling the state of polarized light passing through the LC layer.[71] However, only when the magnetic field reaches a high value does the optical axis of the LC rotate. Therefore, the idea that LCs doped with magnetic components to enhance the

magneto-orientational response was proposed.[72] CNCs would spontaneously self-assemble into a highly ordered chiral LC phase at a proper concentration, enabling to tune the chiral nematic phase under an applied magnetic field. For future application, it is a great challenge to control the CNC assembly under a low magnetic field, needing to induce magnetic domains. As shown in Fig. 4, Zhu *et al.* decorated the CNCs with Fe_3O_4 nanoparticles (Fe_3O_4/CNCs) to improve the magnetic response of the hybrid system, which can tune helical pitch using an ultrasmall magnetic field.[73] Lanceros-Mendez *et al.* reported the straightforward and inexpensive fabrication of the CNC/$CoFe_2O_4$ through evaporation-induced self-assembly using water as the dispersing agent.[74] $CoFe_2O_4$ nanoparticles with high magnetization not only decreased the optical transparency and enhanced thermal stability but also induced a higher magnetization value.

4. Applications

As mentioned above, the construction of a chiral inorganic-doped LC system has turned out to be one of the most effective approaches to introduce, visualize and amplify chirality, enabling them to be the practical candidates for application. Currently, although the study of amplifying inorganic chirality by LCs is just at the infant stage, they are still indispensable parts in many fields, *e.g.*, encryption, sensing, and optics. For encryption, they have been attempted to optical labels; in sensing, they have shown great potential in fluorescent nanosensors used for amino acid and humidity detection; in optics, they are used as array microlens. Herein, we will address the most representative reported examples.

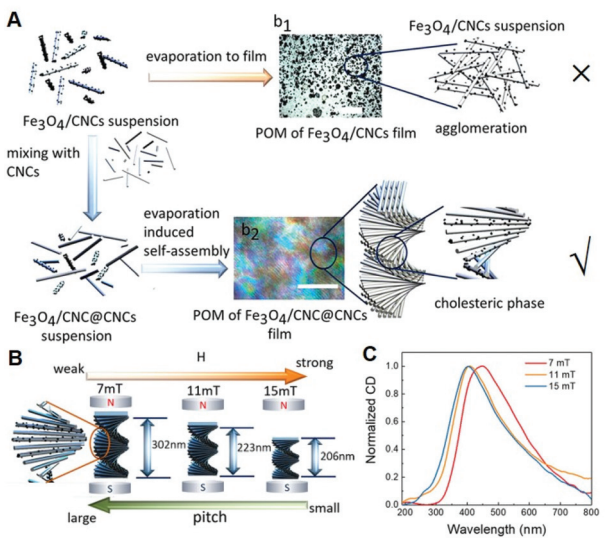

Fig. 4 (A) Synthetic scheme of self-assembly progress of chiral Fe_3O_4/CNC@CNCs films. (B) The relationship between the pitch of chiral structure and the applied magnetic field. (C) CD spectra for Fe_3O_4/CNC@CNCs films with different applied magnetic fields ranging from 7 to 15 mT. Adapted with permission from ref. 73. Copyright 2020, American Chemical Society.

4.1 Encryption

Induced N*LCs with CPL activity are able to reflect CPL in a particular direction, while allowing the transmission of opposite-handed CPL.[75,76] Therefore, constructing an encryption system by utilizing the circular polarization ability of the cholesteric LC films is attractive.[77] For example, Liu *et al.* exhibited an optical coding label and information storage by coupling polyethylene glycol-stabilized ZnS/CdSe QDs with CNC photonic films (Fig. 5).[63] Under the natural light, the QR pattern can be seen clearly when the circularly polarized filter with right handedness was covered, while disappearing under a circularly polarized filter with left handedness because CNC films have the nature to reflect L-CPL and transmit R-CPL. Moreover, when irradiating with UV light, the implied fluorescence was emitted by the QDs from the optical label; the QR code pattern can be seen more clearly under the right-handed circularly polarized filter compared to that under the left-handed one because the transmittance of CNC films for R-CPL was higher.

4.2 Sensing

The stimulus-responsive character of LCs promotes the inheritance of their properties in chiral inorganic-doped LC hybrids. The interactions between the stimulus and chiral components change the chirality, manifesting as the change of *g*-factor and g_{lum} values.[78,79] Typically, CD and CPL spectra enable quantifying the degree of the stimulus. As presented in Fig. 6A, Liu *et al.* fabricated the chiral photonic cellulose film *via* the co-assembly of CNCs, upconversion nanoparticles, and glycerol.[80] As a sensor responded to the humidity when the relative

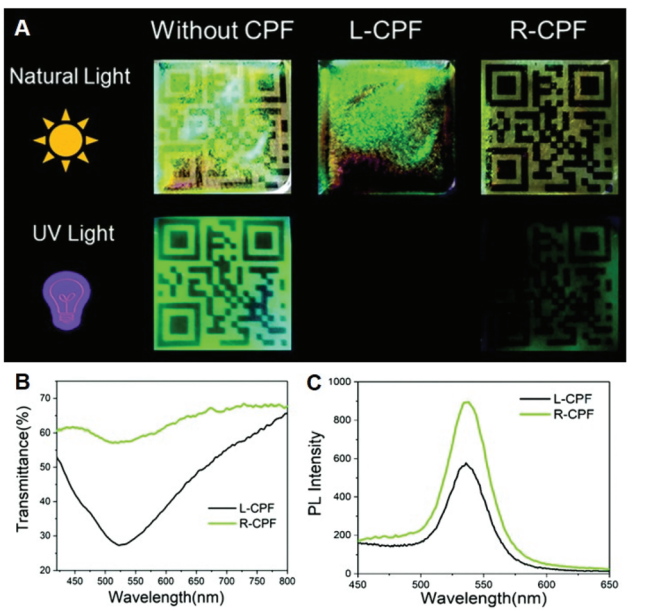

Fig. 5 (A) Photographs of optical coding labels based on the CNC film without or with different-handed circularly polarized filters under natural and UV light. (B) transmittance and (C) Photoluminescence spectra of the CNC films under L- and R-circularly polarized filters. Adapted with permission from ref. 63. Copyright 2019, Royal Society of Chemistry.

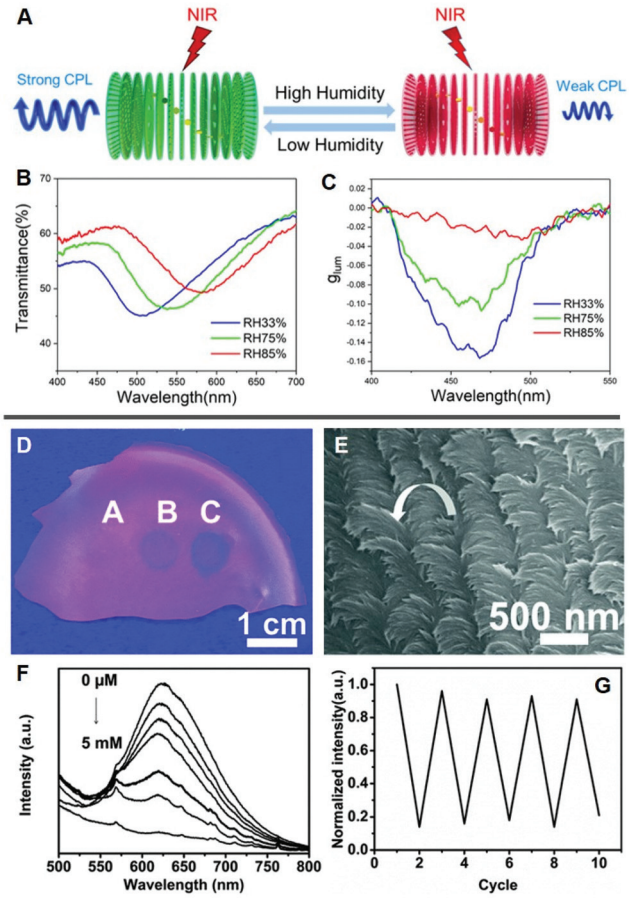

Fig. 6 (A) Illustration of humidity responsive upconverted CPL based on CNC photonic film doped with glycerol. (B) Transmittance spectra and (C) g_{lum} curves of the glycerol laminate film at different relative humidity values. Adapted with permission from ref. 80. Copyright 2019, American Chemical Society. (D) Photograph and (E) SEM image of a $AuNC_4$–CNC film fingerprinted by 2,4,6-trinitrophenol solution. (F) Fluorescence spectrum of the $AuNC_4$–CNC composite film with different 2,4,6-trinitrophenol concentrations. (G) The stability test of the $AuNC_4$–CNC film in ethanol solution. Adapted with permission from ref. 82. Copyright 2016, Royal Society of Chemistry.

humidity increased, the PBG of CNC/glycerol laminate films red-shifted from 505 to 581 nm (Fig. 6B), because of the strong hygroscopicity of glycerol.[81] In the circumstances, the increased L-CPL emission occurring at 450 nm was resulting from the decreased overlap between the PBG and the upconverted emissions at that wavelength and thus causing decreased $|g_{lum}|$ values. In brief, when exposed to different relative humidity, the film exhibited stimuli-responsive upconverted CPL emission with the change of $|g_{lum}|$ values (Fig. 6C).

In addition, the formation of chiral nematic structure can markedly amplify the fluorescence emission, as a consequence, the detection limit is reduced, and the nonlinear response is enhanced. As illustratively shown in Fig. 6D–G, Xu *et al.* reported free-standing fluorescent sensors by embedding gold nanoclusters (AuNCs) in a chiral nematic CNC film.[82] AuNCs–CNC exhibited fluorescence emission with chiroptical-

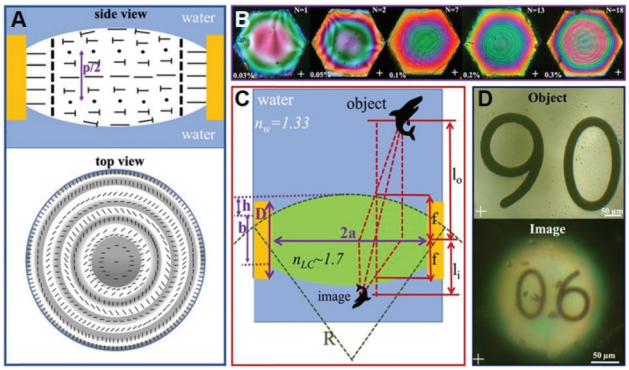

Fig. 7 (A) Side and vertical views of the direction configuration of N*LCs in the lens-shaped droplets. (B) POM images of Au nanoparticles doped N*LCs lenses with different concentrations of Au ranging from 0.03 to 0.3 wt%, which is consistent with the number of fringes ranging between 1 and 18, respectively. (C) The optical ray tracing and the geometry of Au doped N*LC lens. (D) Patterns along with their inverted images at Au-nanoparticles-doped lens. Adapted with permission from ref. 87. Copyright 2021, American Chemical Society.

modulation in the red region through the coupling effect of stopband- and band edge-emission. When the concentration of 2,4,6-trinitrophenol solution added dropwise to the AuNC–CNCs was increased, the clear fingerprint formed on the film became darker under 365 nm UV illumination. The fluorescence quenching was caused by an electronic energy transfer and charge transfer process when the electron-deficient nitroaromatic was exposed to the electron-rich amine-functionalized AuNCs.[83]

4.3 Optics

LCs can be used to create optical lenses by utilizing short helical pitch chiral nematic LC polygonal textures.[84–86] Incorporating the chiral molecules into nematic LCs can lead to the formation of a biconvex lens underwater. For example, Jákli *et al.* used chiral ligand-capped Au nanoparticles doped LCs to spontaneously form converging microlens arrays, as illustratively shown in Fig. 7A–D.[87] When the N*LC film was utterly immersed in water, concentric rings with different background birefringence colors will appear, which indicated the shape of the lens. Meanwhile, when the number of chiral Au nanoparticles increases, the variation of the birefringence colors and the number of rings will increase, which is consistent with the focal lengths of these lenses. Eventually, the patterns as well as their inverted images will be seen.

5. Conclusion and perspectives

In this review, the generation and amplification of inorganic chirality in N*LCs, as well as the current applications are elaborated. When chiral elements are doped, N*LCs will be generated by self-organizing into one-dimension periodic helical structures, manifesting as enhanced chirality. Inorganic nanomaterials with different types will offer unique properties and

universal applicability to diversify chiral materials after combining with LCs. Based on the recent progress, the perspectives about current challenges and future directions in terms of material variety, new synthesis, and future applications of inorganic-doped N*LCs are outlined as follows:

(1) Material variety. Up to date, inorganic materials used as functional components within inorganic-doped N*LC system are mainly non-emissive chiral dopants and emissive achiral dopants. For non-emissive chiral dopants, they are commonly capable of inducing the helical structure in nematic LCs. Whereas for the achiral emitter-N*LC hybrid system, the addition of extra chiral dopants is necessary for the generation of chiral environment. Therefore, developing new chiral inorganic materials with considerable HTP values is still a big challenge. What is more, recent researches are relying on the induced N*LC phase; other LC phases such as chiral smectic-C phase (SmC*), twist-bend nematic (N_{TB}), and blue phase (BP*) are expected to be seen in future investigations.

(2) Novel synthesis strategy. Thermotropic and lyotropic LCs are used as a host to assemble the functionalized inorganic nanomaterials varying in size, aspect ratio, and shape, enabling to control the inorganic location (such as the edge or centre of the PBG) with the formation of helix structure *via* the co-assembling approach. The novel strategies to obtain inorganic-doped N*LCs with considerable chiral transfer efficiency or high g_{lum} values are desired to be explored.

(3) Application. Compared with other chiral structures, the stronger chirality of inorganic-doped N*LCs enables them as proper candidates for practical applications. Despite the fact that the study on amplifying inorganic chirality by LCs is at the infancy stage, they have already become an indispensable part in many fields, *e.g.*, encryption, sensing, and optics. Future efforts in this field need to experience the evolution from fundamental researches to commercial utilizations. When combined with inorganic emitters, extensive CPL signal will appear based on the chiral inorganic-doped LC hybrids, which, we believe, is the best opportunity to realize this transition.

In summary, the combination of inorganic domains and LCs will act as a pivotal part and create vast opportunities in the chiral research field.

Author contributions

T. Z. conceived the idea and supervised the project. M. Z. and Y. W. wrote the paper. T. Z. revised the paper. Y. Z., H. Y. and Q. G. helped to collect the information. All authors discussed the results and assisted during manuscript preparation.

Conflicts of interest

There are no conflicts to declare.

Acknowledgements

This work was supported by the National Natural Science Foundation of China (Grant 22071226) and the Funding of University of Science and Technology of China (Grants KY2060000168, YD2060002013).

Notes and references

1 G. Vulugundam, S. K. Misra, F. Ostadhossein, A. S. Schwartz-Duval, E. A. Daza and D. Pan, *Chem. Commun.*, 2016, **52**, 7513–7516.
2 B. P. Bloom, V. Kiran, V. Varade, R. Naaman and D. H. Waldeck, *Nano Lett.*, 2016, **16**, 4583–4589.
3 H. Maeda, Y. Bando, K. Shimomura, I. Yamada, M. Naito, K. Nobusawa, H. Tsumatori and T. Kawai, *J. Am. Chem. Soc.*, 2011, **133**, 9266–9269.
4 M. Schadt, *Annu. Rev. Mater. Sci.*, 1997, **27**, 305–379.
5 H. Ni, W. L. Chan and Y. Lu, *Chem. Rev.*, 2018, **118**, 9344–9411.
6 W. Ma, L. Xu, A. F. de Moura, X. Wu, H. Kuang, C. Xu and N. A. Kotov, *Chem. Rev.*, 2017, **117**, 8041–8093.
7 L. Xiao, T. An, L. Wang, X. Xu and H. Sun, *Nano Today*, 2020, **30**, 100824.
8 T. T. Zhuang, Y. Li, X. Gao, M. Wei, F. P. Garcia de Arquer, P. Todorovic, J. Tian, G. Li, C. Zhang, X. Li, L. Dong, Y. Song, Y. Lu, X. Yang, L. Zhang, F. Fan, S. O. Kelley, S. H. Yu, Z. Tang and E. H. Sargent, *Nat. Nanotechnol.*, 2020, **15**, 192–197.
9 Y. Sang, J. Han, T. Zhao, P. Duan and M. Liu, *Adv. Mater.*, 2020, **32**, e1900110.
10 X. Han, C. Yuan, B. Hou, L. Liu, H. Li, Y. Liu and Y. Cui, *Chem. Soc. Rev.*, 2020, **49**, 6248–6272.
11 X. Bai, Y. Sun, Y. Jiang, G. Zhao, J. Jiang, C. Yuan and M. Liu, *Angew. Chem., Int. Ed.*, 2021, **60**, 3745–3751.
12 W. Ji, B. Xue, S. Bera, S. Guerin, L. J. W. Shimon, Q. Ma, S. A. M. Tofail, D. Thompson, Y. Cao, W. Wang and E. Gazit, *Mater. Today*, 2021, **42**, 29–40.
13 E. M. Sanchez-Carnerero, F. Moreno, B. L. Maroto, A. R. Agarrabeitia, M. J. Ortiz, B. G. Vo, G. Muller and S. de la Moya, *J. Am. Chem. Soc.*, 2014, **136**, 3346–3349.
14 E. M. Sanchez-Carnerero, A. R. Agarrabeitia, F. Moreno, B. L. Maroto, G. Muller, M. J. Ortiz and S. de la Moya, *Chem. – Eur. J.*, 2015, **21**, 13488–13500.
15 X. Gao, B. Han, X. Yang and Z. Tang, *J. Am. Chem. Soc.*, 2019, **141**, 13700–13707.
16 J. Liu, L. Yang, P. Qin, S. Zhang, K. K. L. Yung and Z. Huang, *Adv. Mater.*, 2021, e2005506, DOI: 10.1002/adma.202005506.
17 X. Shao, Y. Wu, S. Jiang, B. Li, T. Zhang and Y. Yan, *J. Mater. Chem. C*, 2021, **9**, 555–561.
18 V. Kuznetsova, Y. Gromova, M. Martinez-Carmona, F. Purcell-Milton, E. Ushakova, S. Cherevkov, V. Maslov and Y. K. Gun'ko, *Nanophotonics*, 2020, **10**, 797–824.

19 S. Huo, P. Duan, T. Jiao, Q. Peng and M. Liu, *Angew. Chem., Int. Ed.*, 2017, **56**, 12174–12178.
20 K. Ariga, T. Mori, T. Kitao and T. Uemura, *Adv. Mater.*, 2020, **32**, e1905657.
21 J. Lu, Y. Xue, K. Bernardino, N.-N. Zhang, W. R. Gomes, N. S. Ramesar, S. Liu, Z. Hu, T. Sun and A. F. de Moura, *Science*, 2021, **371**, 1368–1374.
22 W. Jiang, Z.-B. Qu, P. Kumar, D. Vecchio, Y. Wang, Y. Ma, J. H. Bahng, K. Bernardino, W. R. Gomes and F. M. Colombari, *Science*, 2020, **368**, 642–648.
23 L. Shi, L. Zhu, J. Guo, L. Zhang, Y. Shi, Y. Zhang, K. Hou, Y. Zheng, Y. Zhu, J. Lv, S. Liu and Z. Tang, *Angew. Chem., Int. Ed.*, 2017, **56**, 15397–15401.
24 Z. Li, Z. Zhu, W. Liu, Y. Zhou, B. Han, Y. Gao and Z. Tang, *J. Am. Chem. Soc.*, 2012, **134**, 3322–3325.
25 I. Lieberman, G. Shemer, T. Fried, E. M. Kosower and G. Markovich, *Angew. Chem., Int. Ed.*, 2008, **47**, 4855–4857.
26 S. Boriskina and N. Zheludev, *Singular and Chiral Nanoplasmonics*, 2014, DOI: 10.1201/b17632.
27 O. Govorov, Z. Fan, P. Hernandez, J. M. Slocik and R. R. Naik, *Nano Lett.*, 2010, **10**, 1374–1382.
28 N. A. Abdulrahman, Z. Fan, T. Tonooka, S. M. Kelly, N. Gadegaard, E. Hendry, A. O. Govorov and M. Kadodwala, *Nano Lett.*, 2012, **12**, 977–983.
29 T. Harada, N. Kajiyama, K. Ishizaka, R. Toyofuku, K. Izumi, K. Umemura, Y. Imai, N. Taniguchi and K. Mishima, *Chem. Commun.*, 2014, **50**, 11169–11172.
30 L. J. Prins, P. Timmerman and D. N. Reinhoudt, *J. Am. Chem. Soc.*, 2001, **123**, 10153–10163.
31 H. Ruan, G. Chen, X. Zhao, Y. Wang, Y. Liao, H. Peng, C. L. Feng, X. Xie and I. I. Smalyukh, *ACS Appl. Mater. Interfaces*, 2018, **10**, 43184–43191.
32 Q. Xia, L. Meng, T. He, G. Huang, B. S. Li and B. Z. Tang, *ACS Nano*, 2021, **15**, 4956–4966.
33 T. Kato, M. Yoshio, T. Ichikawa, B. Soberats, H. Ohno and M. Funahashi, *Nat. Rev. Mater.*, 2017, **2**, 17001.
34 K. Nayani, Y. K. Kim and N. L. Abbott, *Nat. Mater.*, 2017, **17**, 14–15.
35 H. K. Bisoyi and Q. Li, *Acc. Chem. Res.*, 2014, **47**, 3184–3195.
36 X. Yang, X. Jin, T. Zhao and P. Duan, *Mater. Chem. Front.*, 2021, **5**, 4821–4832.
37 H. K. Bisoyi and Q. Li, *Angew. Chem., Int. Ed.*, 2016, **55**, 2994–3010.
38 B. A. San Jose, S. Matsushita and K. Akagi, *J. Am. Chem. Soc.*, 2012, **134**, 19795–19807.
39 D. P. N. Gonçalves, M. E. Prévôt, Ş. Üstünel, T. Ogolla, A. Nemati, S. Shadpour and T. Hegmann, *Liq. Cryst. Rev.*, 2021, **9**, 1–34.
40 R. Eelkema and B. L. Feringa, *Org. Biomol. Chem.*, 2006, **4**, 3729–3745.
41 G. Pathak, G. Hegde and V. Prasad, *Liq. Cryst.*, 2020, **48**, 579–587.
42 M. Xu, X. Wu, Y. Yang, C. Ma, W. Li, H. Yu, Z. Chen, J. Li, K. Zhang and S. Liu, *ACS Nano*, 2020, **14**, 11130–11139.
43 A. Nemati, S. Shadpour, L. Querciagrossa, L. Li, T. Mori, M. Gao, C. Zannoni and T. Hegmann, *Nat. Commun.*, 2018, **9**, 3908.
44 A. L. Rodarte, C. Gray, L. S. Hirst and S. Ghosh, *Phys. Rev. B: Condens. Matter Mater. Phys.*, 2012, **85**, 035430.
45 M. Mitov, *Adv. Mater.*, 2012, **24**, 6260–6276.
46 J. Yan, F. Ota, B. A. San Jose and K. Akagi, *Adv. Funct. Mater.*, 2017, **27**, 1604529.
47 M. Mathews, R. S. Zola, S. Hurley, D.-K. Yang, T. J. White, T. J. Bunning and Q. Li, *J. Am. Chem. Soc.*, 2010, **132**, 18361–18366.
48 Y. Wang and Q. Li, *Adv. Mater.*, 2012, **24**, 1926–1945.
49 M. Goh, M. Kyotani and K. Akagi, *J. Am. Chem. Soc.*, 2007, **129**, 8519–8527.
50 S. Dussi and M. Dijkstra, *Nat. Commun.*, 2016, **7**, 11175.
51 H. B. Kolli, G. Cinacchi, A. Ferrarini and A. Giacometti, *Faraday Discuss.*, 2016, **186**, 171–186.
52 T. Mori, A. Sharma and T. Hegmann, *ACS Nano*, 2016, **10**, 1552–1564.
53 A. Sharma, T. Mori, H.-C. Lee, M. Worden, E. Bidwell and T. Hegmann, *ACS Nano*, 2014, **12**, 11966–11976.
54 A. Guerrero-Martinez, B. Auguie, J. L. Alonso-Gomez, Z. Dzolic, S. Gomez-Grana, M. Zinic, M. M. Cid and L. M. Liz-Marzan, *Angew. Chem., Int. Ed.*, 2011, **50**, 5499–5503.
55 F. P. Garcia de Arquer, D. V. Talapin, V. I. Klimov, Y. Arakawa, M. Bayer and E. H. Sargent, *Science*, 2021, **373**, 6555.
56 Y. Zhou, R. L. Marson, G. van Anders, J. Zhu, G. Ma, P. Ercius, K. Sun, B. Yeom, S. C. Glotzer and N. A. Kotov, *ACS Nano*, 2016, **10**, 3248–3256.
57 J. Schneider, W. Zhang, A. K. Srivastava, V. G. Chigrinov, H. S. Kwok and A. L. Rogach, *Nano Lett.*, 2017, **17**, 3133–3138.
58 A. Bobrovsky, K. Mochalov, V. Oleinikov and V. Shibaev, *Liq. Cryst.*, 2011, **38**, 737–742.
59 A. Bobrovsky, K. Mochalov, V. Oleinikov, A. Sukhanova, A. Prudnikau, M. Artemyev, V. Shibaev and I. Nabiev, *Adv. Mater.*, 2012, **24**, 6216–6222.
60 H. K. Bisoyi, T. J. Bunning and Q. Li, *Adv. Mater.*, 2018, **30**, e1706512.
61 L. Chen, C. Lai, R. Marchewka, R. M. Berry and K. C. Tam, *Nanoscale*, 2016, **8**, 13288–13296.
62 U. Ngoensawat, A. Parnsubsakul, S. Kaitphaiboonwet, T. Wutikhun, C. Sapcharoenkun, P. Pienpinijtham and S. Ekgasit, *Carbohydr. Polym.*, 2021, **262**, 117864.
63 M. Xu, C. Ma, J. Zhou, Y. Liu, X. Wu, S. Luo, W. Li, H. Yu, Y. Wang, Z. Chen, J. Li and S. Liu, *J. Mater. Chem. C*, 2019, **7**, 13794–13802.
64 Y. Shi, Z. Zhou, X. Miao, Y. J. Liu, Q. Fan, K. Wang, D. Luo and X. W. Sun, *J. Mater. Chem. C*, 2020, **8**, 1048–1053.
65 J. Ma, H. Wang and D. Li, *Adv. Mater.*, 2021, **33**, e2008785.
66 I. Infante and L. Manna, *Nano Lett.*, 2021, **21**, 6–9.
67 L.-Q. Lu, M.-Y. Ma, T. Tan, X.-K. Tian, Z.-X. Zhou, C. Yang and Y. Li, *Sens. Actuators, B*, 2018, **270**, 291–297.

68 C. T. Wang, K. Chen, P. Xu, F. Yeung, H. S. Kwok and G. Li, *Adv. Funct. Mater.*, 2019, **29**, e1903155.
69 T. Zhao, J. Han, P. Duan and M. Liu, *Acc. Chem. Res.*, 2020, **53**, 1279–1292.
70 X. Yang, M. Zhou, Y. Wang and P. Duan, *Adv. Mater.*, 2020, **32**, e2000820.
71 B. Frka-Petesic, J. Sugiyama, S. Kimura, H. Chanzy and G. Maret, *Macromolecules*, 2015, **48**, 8844–8857.
72 L. Zadoina, B. Lonetti, K. Soulantica, A. F. Mingotaud, M. Respaud, B. Chaudret and M. Mauzac, *J. Mater. Chem.*, 2009, **19**, 8075–8078.
73 T. Chen, Q. Zhao, X. Meng, Y. Li, H. Peng, A. K. Whittaker and S. Zhu, *ACS Nano*, 2020, **14**, 9440–9448.
74 E. Lizundia, A. Maceiras, J. L. Vilas, P. Martins and S. Lanceros-Mendez, *Carbohydr. Polym.*, 2017, **175**, 425–432.
75 X. Yang, J. Han, Y. Wang and P. Duan, *Chem. Sci.*, 2019, **10**, 172–178.
76 D. Han, X. Yang, J. Han, J. Zhou, T. Jiao and P. Duan, *Nat. Commun.*, 2020, **11**, 5659.
77 R. Liu, B. Ding, D. Liu and X. Ma, *Chem. Eng. J.*, 2021, **421**, 129732.
78 E. Zor, H. Bingol and M. Ersoz, *TrAC, Trends Anal. Chem.*, 2019, **121**, 115662.
79 Z. Li, J. Lu, L. Jin, J. Rusz, V. Kocevski, H. Yanagihara, E. Kita, J. Mayer, R. E. Dunin-Borkowski, H. Xiang and X. Zhong, *Adv. Funct. Mater.*, 2021, **31**, e2008306.
80 W. Li, M. Xu, C. Ma, Y. Liu, J. Zhou, Z. Chen, Y. Wang, H. Yu, J. Li and S. Liu, *ACS Appl. Mater. Interfaces*, 2019, **11**, 23512–23519.
81 M. Xu, W. Li, C. Ma, H. Yu, Y. Wu, Y. Wang, Z. Chen, J. Li and S. Liu, *J. Mater. Chem. C*, 2018, **6**, 5391–5400.
82 D. Qu, J. Zhang, G. Chu, H. Jiang, C. Wu and Y. Xu, *J. Mater. Chem. C*, 2016, **4**, 1764–1768.
83 Y. Ma, H. Li, S. Peng and L. Wang, *Anal. Chem.*, 2012, **84**, 8415–8421.
84 P. Popov, L. W. Honaker, M. Mirheydari, E. K. Mann and A. Jakli, *Sci. Rep.*, 2017, **7**, 1603.
85 Y. Li, Y. Liu and D. Luo, *J. Mater. Chem. C*, 2019, **7**, 15166–15170.
86 Y. Ke, Y. Liu, J. Zhou, Y. Liu, H. Luo and S. Wen, *Appl. Phys. Lett.*, 2016, **108**, 101102.
87 K. Perera, A. Nemati, E. K. Mann, T. Hegmann and A. Jákli, *ACS Appl. Mater. Interfaces*, 2021, **13**, 4574–4582.